Exploring differential two-particle correlations in γp and low-multiplicity pp collisions using PYTHIA8

Subash Chandra Behera[1,*] and Dukhishyam Mallick[2,†]
[1]*INFN–Sezione di Roma, Piazzale Aldo Moro, 2-00185 Rome, Italy*
[2]*INFN–Sezione di Cagliari, Monserrato, 09042, Cagliari, Italy*

(Received 23 February 2026; accepted 7 October 2026; published 26 October 2026)

A study of two-particle differential number (B) and transverse momentum (P_2^{CD}) balance functions in photon-proton (γp) and proton-proton (pp) collisions at $\sqrt{s} = 5.36$ TeV is presented. The analysis focuses on inclusive charged hadrons within the pseudorapidity coverage $|\eta| < 2.4$ and the transverse momentum interval $0.3 < p_{\mathrm{T}} < 3.0$ GeV and examines their correlations in terms of relative pseudorapidity ($\Delta\eta$) and relative azimuthal angle ($\Delta\phi$). The correlation functions are evaluated for same- and opposite-sign pairs, and their combinations are used to extract charge-dependent (CD) and charge-independent (CI) components. The evolution of the nearside peak of the CD correlations is investigated in terms of $\Delta\eta$ and $\Delta\phi$ as a function of charged-particle multiplicity (N_{ch}) for γp collisions and compared to pp collisions at a similar multiplicity range. A clear multiplicity dependence of the balance-function width is obtained. The width is found systematically lower in γp events than in pp collisions. This study provides valuable information on particle correlations and production mechanisms in low-N_{ch} regimes for upcoming measurements in small systems.

DOI: 10.1103/fq2g-2vz2

I. INTRODUCTION

Measurements from ultrarelativistic heavy-ion collisions at the Relativistic Heavy Ion Collider (RHIC) and the Large Hadron Collider (LHC) have provided compelling evidence for the formation of a strongly interacting matter known as the quark-gluon plasma (QGP) [1–7].

The observation of collective flow, especially the large elliptic flow coefficient (v_2), and its comparison with theoretical calculations based on relativistic hydrodynamics suggests that the QGP behaves like an almost perfect fluid with extremely low shear viscosity. In particular, the large value of v_2 is found to be consistent with a medium having a very small shear viscosity to entropy density ratio, $4\pi\eta/s \sim 1$–2, close to the conjectured lower bound for a strongly coupled fluid [8,9]. Studying correlations between oppositely charged particle pairs created in heavy-ion collisions provides insight into the dynamics of the QGP and the underlying hadronization mechanism [10–18]. The particle production is governed by local charge conservation, in which the creation of a positively charged particle must be accompanied by the production of a negatively charged partner. The balance function is designed to quantify the correlations in phase space variables such as pseudorapidity difference ($\Delta\eta$) and azimuthal angle difference ($\Delta\phi$) [11–14,16,19–23].

Measurements of the nearside peak width of the charge balance function exhibit a strong system-size dependence across various collision systems spanning RHIC to LHC energies [17–20]. A significant narrowing of the balance functions width is observed in central heavy-ion collisions. This effect is interpreted as the signature of delayed hadronization in the presence of the QGP medium, where balancing charges are produced at a later stage of the system evolution and therefore remain closer in phase space [17–20].

Recent observations of long-range rapidity correlations ("ridgelike" structures), nonzero flow harmonics, and the narrowing of the nearside width of the correlation functions in small collision systems exhibit features qualitatively similar to those seen in heavy-ion collisions [3,24–28]. The unexpected narrowing behavior challenges the conventional interpretation associated with delayed hadronization in the deconfined medium. As a result, the mechanism responsible for this behavior in small systems remains not fully understood [25,28,29].

Several theoretical studies using event generators such as PYTHIA, AMPT, and EPOS, which incorporate distinct physics mechanisms including string fragmentation, partonic transport, and hydrodynamic evolution, also reproduce the

*Contact author: subash.chandra.behera@cern.ch
†Contact author: dukhishyam.mallick@cern.ch

Published by the American Physical Society under the terms of the Creative Commons Attribution 4.0 International license. Further distribution of this work must maintain attribution to the author(s) and the published article's title, journal citation, and DOI.

similar decreasing trend of the balance-function width with increasing multiplicity [14,19,30–32]. This suggests that multiple mechanisms, such as local charge conservation, string dynamics, multiple parton interactions (MPIs), color reconnection (CR), or parton transport effects, may contribute to the observed behavior.

In this work, the correlation functions are further investigated in even smaller collision systems, extending to photon-induced γp collisions using PYTHIA 8 simulations [33,34]. Such collisions provide a cleaner environment compared to hadronic pp interactions, as electromagnetic processes dominate and the underlying hadronic event activity is significantly suppressed [35,36]. These events are characterized by very low charged-particle multiplicity due to the suppression of the MPI and the absence of an extended QGP-like medium. Therefore, γp collisions offer an ideal baseline for studying correlation functions and disentangling genuine charge conservation effects from medium-induced phenomena observed in hadronic collisions.

In this work, both charge-independent (CI) and charge-dependent (CD) two-particle number and transverse-momentum (p_{T}) correlations are presented. The focus of this study is the CD correlation, which isolates correlations associated with charge conservation by subtracting same-sign (SS) pair contributions from opposite-sign (OS) pairs. Then, to quantify the correlation strength, the root-mean-square (RMS) widths of the CD correlation functions are extracted from their one-dimensional distributions onto $\Delta\eta$ and $\Delta\phi$.

This paper is organized as follows. Section II describes the analysis methodology. Section III discusses the model setup and framework used for this study. Section IV presents the results for B, P_2^{CD} correlations, and their corresponding widths in $\Delta\eta$ and $\Delta\phi$. Finally, Sec. V summarizes this work. Additional discussions about the CI correlations can be found in Sec. VI.

II. ANALYSIS METHODOLOGY

Two-particle number correlation functions C_2 are constructed using the "trigger" and "associated" tracks that are selected from the same event. Both the trigger and associated particles are selected in $|\eta| < 2.4$ and $0.3 < p_{\mathrm{T}} < 3.0$ GeV intervals. For each pair, the differences in $\Delta\eta$ and $\Delta\phi$ are calculated. The per-trigger associated yield in the same event is defined as

$$S(\Delta\eta,\Delta\phi) = \frac{1}{N_{\mathrm{trig}}}\frac{d^2N^{\mathrm{same}}}{d\Delta\eta d\Delta\phi}, \tag{1}$$

where N_{trig} is the number of trigger particles and N^{same} is the number of same-event pairs. The mixed-event distributions are calculated by randomly mixing six chosen events in the similar multiplicity class for $0.3 < p_{\mathrm{T}} < 3.0$ GeV and $|\eta| < 2.4$ intervals. This can be written as

$$M(\Delta\eta,\Delta\phi) = \frac{1}{N_{\mathrm{trig}}}\frac{d^2N^{\mathrm{mix}}}{d\Delta\eta d\Delta\phi}, \tag{2}$$

where N^{mix} denotes the number of mixed-event pairs. The mixed-event background distribution accounts for the finite detector acceptance and pair efficiency [19,20,24,26,27,30,35]. The two-particle number correlation function is then obtained as the ratio of the same-event signal to the mixed-event background [19,20,24,26,27,30,35].

$$\frac{1}{N_{\mathrm{trig}}}\frac{d^2N^{\mathrm{pair}}}{d\Delta\eta d\Delta\phi} = C_2(\Delta\eta,\Delta\phi) \tag{3}$$

$$= M(0,0)\frac{S(\Delta\eta,\Delta\phi)}{M(\Delta\eta,\Delta\phi)}, \tag{4}$$

where the term $M(0,0)/M(\Delta\eta,\Delta\phi)$ mainly accounts for the pair acceptance effects and $M(0,0)$ denotes the mixed-event yield when both particles are emitted approximately in the same direction, leading to the highest pair detection efficiency.

Similarly, the two-particle transverse momentum correlator, P_2, that takes care of p_{T} fluctuations can be defined as

$$P_2(\Delta\eta,\Delta\phi) = \frac{\langle\Delta p_{\mathrm{T}}\Delta p_{\mathrm{T}}\rangle(\Delta\eta,\Delta\phi)}{\langle p_{\mathrm{T}}\rangle^2}, \tag{5}$$

where $\Delta p_{\mathrm{T}} = p_{\mathrm{T}} - \langle p_{\mathrm{T}}\rangle$ and $\langle\Delta p_{\mathrm{T}}\Delta p_{\mathrm{T}}\rangle$ is the differential correlator that can be defined as

$$\langle\Delta p_T\Delta p_T\rangle(\Delta\eta,\Delta\phi) = \frac{\int_{p_{\mathrm{T,min}}}^{p_{\mathrm{T,max}}}\Delta p_{\mathrm{T}}\Delta p_{\mathrm{T}}c_2'(\vec{p}_1,\vec{p}_2)dp_{\mathrm{T}}dp_{\mathrm{T}}}{\int_{p_{\mathrm{T,min}}}^{p_{\mathrm{T,max}}}c_2'(\vec{p}_1,\vec{p}_2)dp_{\mathrm{T}}dp_{\mathrm{T}}}, \tag{6}$$

where c_2' is the two-particle density distribution expressed as a function of the transverse momenta. The momentum correlator is normalized $\langle p_{\mathrm{T}}\rangle^2$ to make the P_2 correlation dimensionless. The P_2 correlation is influenced by the presence of number correlations and the transverse momentum distribution of the correlated particle pairs, and the details can be found in Refs. [15,16,30].

The CI and CD components are constructed using C_2 and P_2 correlation functions from their corresponding SS and OS pairs. The CI correlation is the average of SS and OS correlation functions, and the CD correlation is the difference of the SS and OS correlation functions. The SS and OS pairs are influenced by different physical mechanisms; taking their combination can isolate the correlation associated with balancing charges. This effect is quantified through the CD correlation. Mathematically, these components are expressed as follows:

$$C_2^{\mathrm{CI}} = \frac{1}{2}\left[C_2^{(+,-)} + C_2^{(-,+)} + C_2^{(-,-)} + C_2^{(+,+)}\right], \tag{7}$$

$$P_2^{\mathrm{CI}} = \frac{1}{2}\left[P_2^{(+,-)} + P_2^{(-,+)} + P_2^{(-,-)} + P_2^{(+,+)}\right], \quad (8)$$

$$B = \frac{1}{2}\left[C_2^{(+,-)} + C_2^{(-,+)} - C_2^{(-,-)} - C_2^{(+,+)}\right], \quad (9)$$

$$P_2^{\mathrm{CD}} = \frac{1}{2}\left[P_2^{(+,-)} + P_2^{(-,+)} - P_2^{(-,-)} - P_2^{(+,+)}\right]. \quad (10)$$

The strength of the balance functions is quantified by the RMS value of their one-dimensional (1D) distributions of $\Delta\eta$ and $\Delta\phi$. The 1D $\Delta\eta$ and $\Delta\phi$ projections are obtained from the two-dimensional correlation functions by integrating over the intervals $|\Delta\phi| < \pi/2$ and $|\Delta\eta| < 1.0$, respectively. Mathematically, the RMS width ($\sigma_{\mathcal{O}}$) is defined as follows:

$$\sigma_{\mathcal{O}} = \sqrt{\frac{\sum_i \mathcal{O}_i^2 B(\mathcal{O}_i)}{\sum_i B(\mathcal{O}_i)}}, \quad (11)$$

where $B(\mathcal{O}_i)$ denotes the balance function evaluated in the ith bin centered at $\mathcal{O}_i$, and $\mathcal{O}$ represents the relative separation variable, such as $\Delta\eta$ or $\Delta\phi$. The summation runs over all bins within the selected kinematic range. A similar approach is followed to extract the RMS width of P_2^{CD} correlations. The $\sigma_{\Delta\eta}$ and $\sigma_{\Delta\phi}$ are calculated in $|\Delta\eta| < 2.0$ and $|\Delta\phi| < \pi/2$ intervals, respectively.

III. MODEL DESCRIPTION

In this study, events are generated using PYTHIA 8.36 [33,37] to simulate both γp and pp collisions, with approximately 0.2×10^9 and 3×10^9 events, respectively. For γp collisions, the photon flux is modeled using the equivalent photon approximation implemented in PYTHIA, where the photon is treated as another beam particle (`Beams:idA = 22`). The details of the modeling can be found in Ref. [38].

To provide a realistic description of photon-induced interactions and to suppress contributions from underlying-event activity and MPI, all hard QCD processes are disabled (`HardQCD:all = off`, `PartonLevel:MPI = off`), while photon-induced processes are enabled (`PhotonParton:all = on`). These settings are considered as the default tune for γp collisions. In addition, the Monash tune for minimum-bias (MB) inelastic pp collisions at LHC energies is considered for comparison. The same tune is also applied to the γp simulations to study the differences in final-state particle production and production mechanisms when changing the collision system from pp to γp.

This configuration uses the following tunes: `Tune:pp = 14`, (Monash) `SoftQCD:inelastic = on`, `PartonLevel:MPI = on`, and `ColourReconnection: reconnect = on`. This setup is referred to as the MB-like tune throughout this paper.

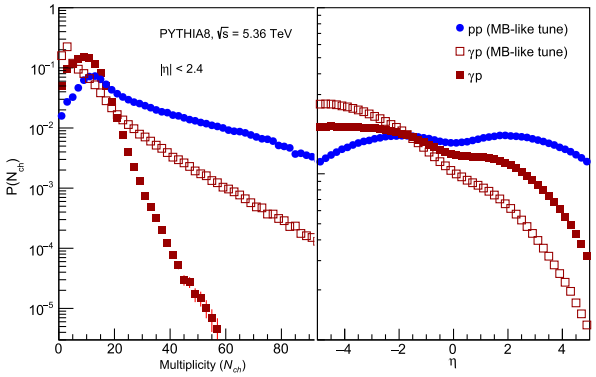


FIG. 1. Comparison of multiplicity (N_{ch}) and pseudorapidity (η) distributions of charged hadrons in MB pp, MB-like tune γp, and γp collisions at $\sqrt{s} = 5.36$ TeV.

Figure 1 illustrates the normalized charged-particle multiplicity (N_{ch}, left panel) and pseudorapidity (η, right panel) distributions in pp and γp collisions from PYTHIA 8 simulations. The charged-particle multiplicity distributions for MB inelastic pp collisions show significantly higher values of N_{ch} compared to γp collisions. The distributions are evaluated within the pseudorapidity interval $|\eta| < 2.4$. The ordering of the multiplicity spectra is observed as

$$N_{\mathrm{ch}}^{\gamma p} < N_{\mathrm{ch}}^{\gamma p,\,\mathrm{MB\text{-}like}} < N_{\mathrm{ch}}^{pp,\,\mathrm{MB\text{-}like}}. \quad (12)$$

The MB pp collisions reach larger N_{ch} values and exhibit broader multiplicity distribution due to the presence of multiple partonic interactions, underlying event activities, and the larger available phase space in a fully hadronic collision system. In contrast, the γp collisions show lower multiplicity coverage and a rapidly falling distribution with increasing N_{ch}. This behavior reflects that the particle production in photon-induced interactions is typically driven by a single hard or semihard scattering process, although the overall N_{ch} not only depends on the colliding systems and energies but is also sensitive to the choice of tunes and underlying physics processes that are included in the simulation.

The η distributions are symmetric around midrapidity ($\eta \sim 0$) in pp collisions, whereas an asymmetric shape is observed in γp collisions. It is expected due to the γp configuration. The multiplicity coverage for this study is chosen based on the maximum N_{ch} reach in γp, and an equivalent multiplicity range is selected for pp collisions.

Figure 2 presents the average transverse momentum ($\langle p_{\mathrm{T}} \rangle$) as a function of the N_{ch} for γp and pp collisions at $\sqrt{s} = 5.36$ TeV from PYTHIA 8 simulations. The $\langle p_{\mathrm{T}} \rangle$ are calculated for charged hadrons in the interval $0.3 < p_{\mathrm{T}} < 3.0$ GeV and within $|\eta| < 2.4$. A monotonically increasing behavior of $\langle p_{\mathrm{T}} \rangle$ with N_{ch} is observed. The $\langle p_{\mathrm{T}} \rangle$ values and

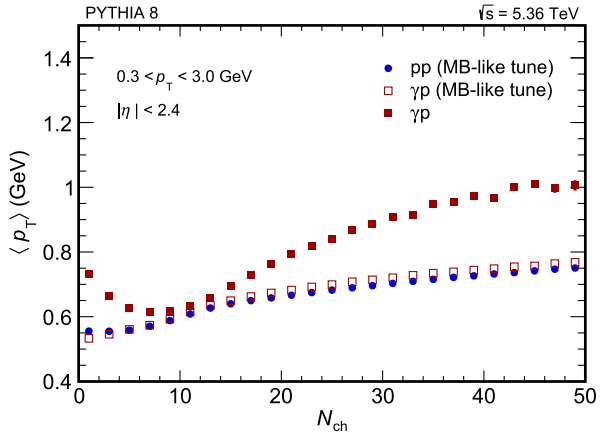


FIG. 2. Comparison of average transverse momentum ($\langle p_{\mathrm{T}} \rangle$) as a function of N_{ch} for charged hadrons in MB pp, MB-like tune γp, and γp collisions at $\sqrt{s} = 5.36$ TeV. Results are calculated for $|\eta| < 2.4$ and $0.3 < p_{\mathrm{T}} < 3.0$ GeV.

their dependence on N_{ch} are found to be similar between γp and pp collisions when they have MB-like configurations. However, a steeper rise of $\langle p_{\mathrm{T}} \rangle$ with N_{ch} is observed for γp collisions with a more realistic configuration for photon-induced interaction. The $\langle p_{\mathrm{T}} \rangle$ values are higher compared to pp collisions at a given multiplicity, and the difference becomes more pronounced at higher N_{ch}. This indicates that the $\langle p_{\mathrm{T}} \rangle$ is more sensitive to the underlying physics processes and model tunes than to the nature of the colliding systems when comparing pp and γp collisions. These results demonstrate that the correlation between multiplicity and transverse momentum depends on several components, such as the roles of quark- and gluon-initiated interactions, color reconnection, and MPI dynamics.

IV. RESULTS AND DISCUSSION

A. Charge-dependent correlations

Figure 3 presents the two-dimensional balance function B for charged hadrons in terms of $\Delta\eta$ and $\Delta\phi$ for two different multiplicity intervals in γp and pp collisions at $\sqrt{s} = 5.36$ TeV. The low and high multiplicities correspond to $0 < N_{\mathrm{ch}} < 5$ (upper panels) and $40 < N_{\mathrm{ch}} < 50$ (lower panels), respectively.

At very low multiplicity ($0 < N_{\mathrm{ch}} < 5$) in pp and MB-like tune γp collisions, the balance function exhibits a strong away-side correlation around $\Delta\phi \approx \pi$, reflecting the dominance of a single hard parton scattering and the resulting back-to-back dijet topology. As the multiplicity increases, this away-side structure decreases in magnitude due to the growing importance of MPI, while the nearside peak at $\Delta\eta \approx 0$ becomes significantly stronger, rising from about 0.01 at $N_{\mathrm{ch}} \approx 5$ to approximately 0.1 for $40 < N_{\mathrm{ch}} < 50$. This behavior is consistent with a transition from long-range charge balancing across dijet events at low multiplicity to predominantly local charge conservation (LCC) at higher multiplicity.

However, the results from the γp collisions (top, right) without MB-like tune of Fig. 3 exhibit different behavior

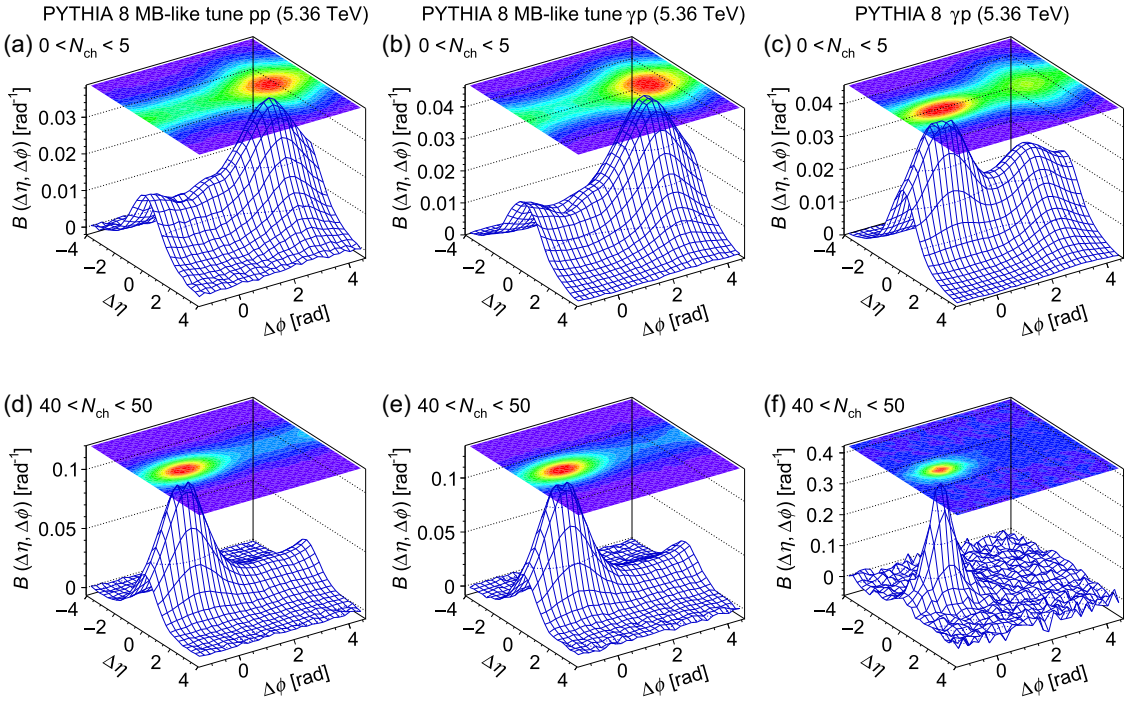


FIG. 3. Two-dimensional number balance functions (B) for $0 < N_{\mathrm{ch}} < 5$ (upper panel) and $40 < N_{\mathrm{ch}} < 50$ (lower panel) of charged hadrons in MB-like tune pp (left), MB-like tune γp (middle), and γp (right) collisions at $\sqrt{s} = 5.36$ TeV from PYTHIA 8. The results are obtained in the kinematic region $|\eta| < 2.4$ and $0.3 < p_{\mathrm{T}} < 3.0$ GeV.

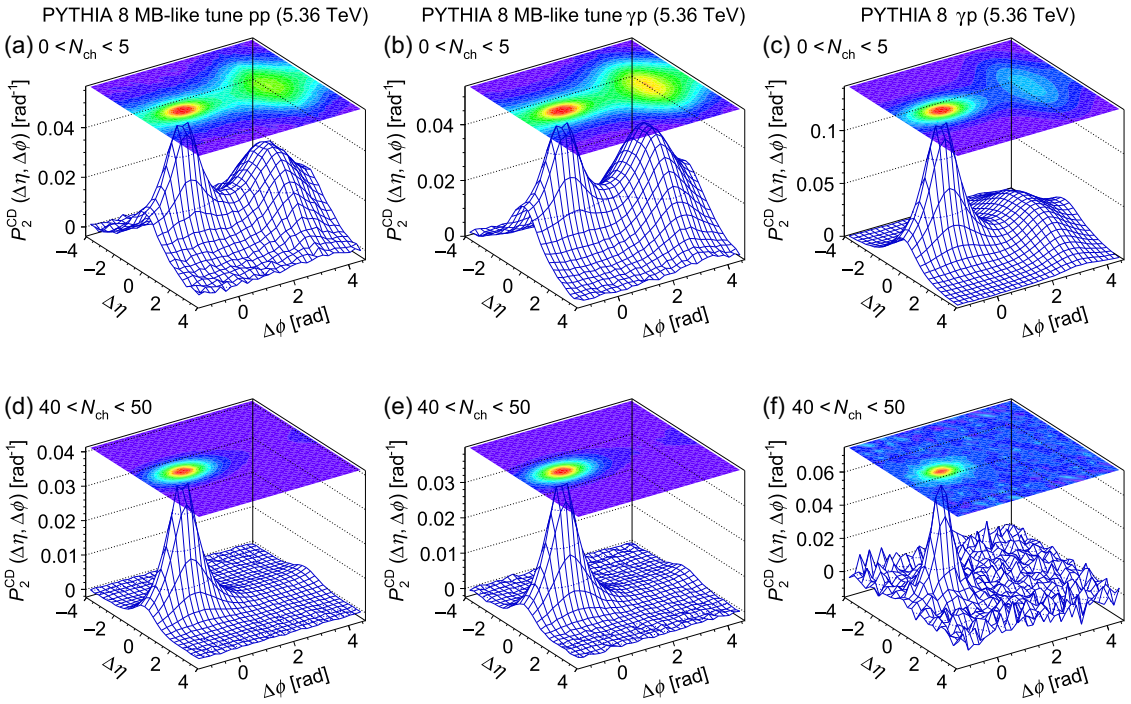


FIG. 4. Two-dimensional momentum balance functions (P_2^{CD}) for $0 < N_{\mathrm{ch}} < 5$ (upper panel) and $40 < N_{\mathrm{ch}} < 50$ (lower panel) of charged hadrons in MB-like tune pp (left), MB-like tune γp (middle), and γp (right) collisions at $\sqrt{s} = 5.36$ TeV from PYTHIA 8. The results are obtained in the kinematic region $|\eta| < 2.4$ and $0.3 < p_{\mathrm{T}} < 3.0$ GeV.

compared to the pp collisions at similar N_{ch}. At very low multiplicity, the B shows a much weaker away-side peak, which rapidly disappears with increasing multiplicity. This suppression is attributed to the lack of MPI and hard QCD dijet contributions because the photon interacts predominantly through a single, highly asymmetric color string attached to a quark in the proton.

At the same time, the amplitude B shows a stronger nearside peak in the γp collisions than pp at the similar N_{ch}. The amplitude changes approximately 0.04 to 0.4 from low to high N_{ch}. This enhanced nearside peak in γp collisions originates from the fact that the charge production is governed almost exclusively by a single, short string with strong local charge ordering. In the absence of MPI, minijets, and multiple color strings, the charge-balancing partners remain tightly correlated in $\Delta\eta$ and $\Delta\phi$ phase space.

Similarly, the two-dimensional charge-dependent momentum balance correlation $P_2^{\mathrm{CD}}(\Delta\eta, \Delta\phi)$ is shown in Fig. 4. A distinct feature is seen when comparing pp and γp collisions. At very low N_{ch}, the nearside peak is significantly stronger in γp interactions than in pp events. This enhancement originates from the single-string topology in γp collisions, where opposite-charge particles are produced in a more localized manner along the string, resulting in tighter momentum correlations.

Interestingly, the away-side correlation $\Delta\phi \approx \pi$ is observed to have similar strength in both systems within the same multiplicity interval. As the event multiplicity increases toward $N_{\mathrm{ch}} \approx 50$, the nearside peak, the strengths converge to similar levels between pp and γp collisions. The results from the γp collisions with the MB-like tune exhibit qualitatively similar behavior to that observed in the pp collisions. It is found that the B and P_2^{CD} observables show similar multiplicity dependence, indicating that they depend more strongly on the underlying processes than the nature of the colliding system.

Overall, a narrower nearside structure in P_2^{CD} relative to B indicates that balancing charges originating from harder partonic processes, such as jet fragmentation, exhibit stronger localized momentum correlations. This difference highlights the sensitivity of these observables to both the topology and the dynamical properties of particle production.

In addition to the CD correlations, a brief discussion about the CI correlations is provided in Sec. VI (Appendix).

B. One-dimensional projections

A clear multiplicity dependence is observed in the 1D distributions of B as a function of $\Delta\eta$ and $\Delta\phi$ for three N_{ch} intervals in pp and γp collisions, as shown in Fig. 5. The nearside peak of the 1D B distribution becomes narrower with increasing N_{ch}. This narrowing is more pronounced in γp compared to pp collisions. Interestingly, the nearside peak of $B(\Delta\phi)$ is nearly flat in pp, but a smaller peaklike structure is seen for the γp at the low N_{ch} region. However, at higher N_{ch}, a sharper peak is found in γp than pp collisions.

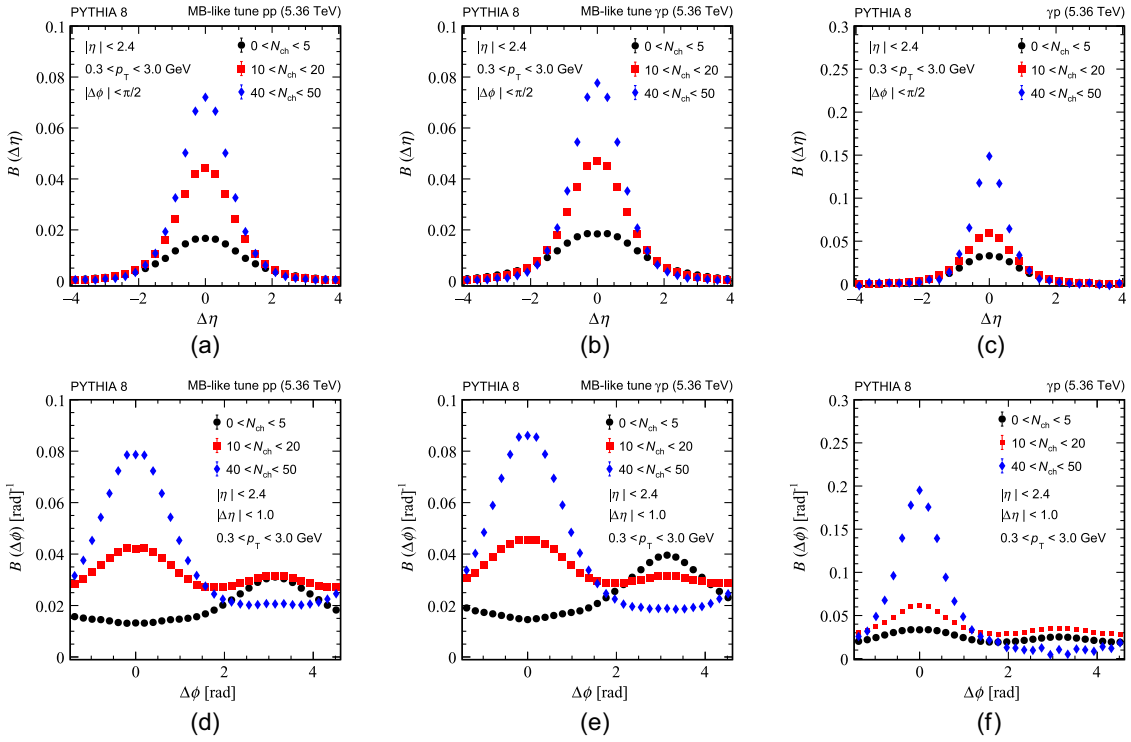


FIG. 5. One-dimensional nearside projection of the number balance functions (B) as a function of $\Delta\eta$ (upper panels) and $\Delta\phi$ (lower panels) for three $N_{\rm ch}$ classes in MB-like tune pp (left panels, (a) and (d)), MB-like tune γp (middle panels, (b) and (e)), and γp (right panels, (c) and (f)) collisions at $\sqrt{s} = 5.36$ TeV from PYTHIA 8. The results are obtained in the kinematic region $|\eta| < 2.4$ and $0.3 < p_{\rm T} < 3.0$ GeV for charged hadrons.

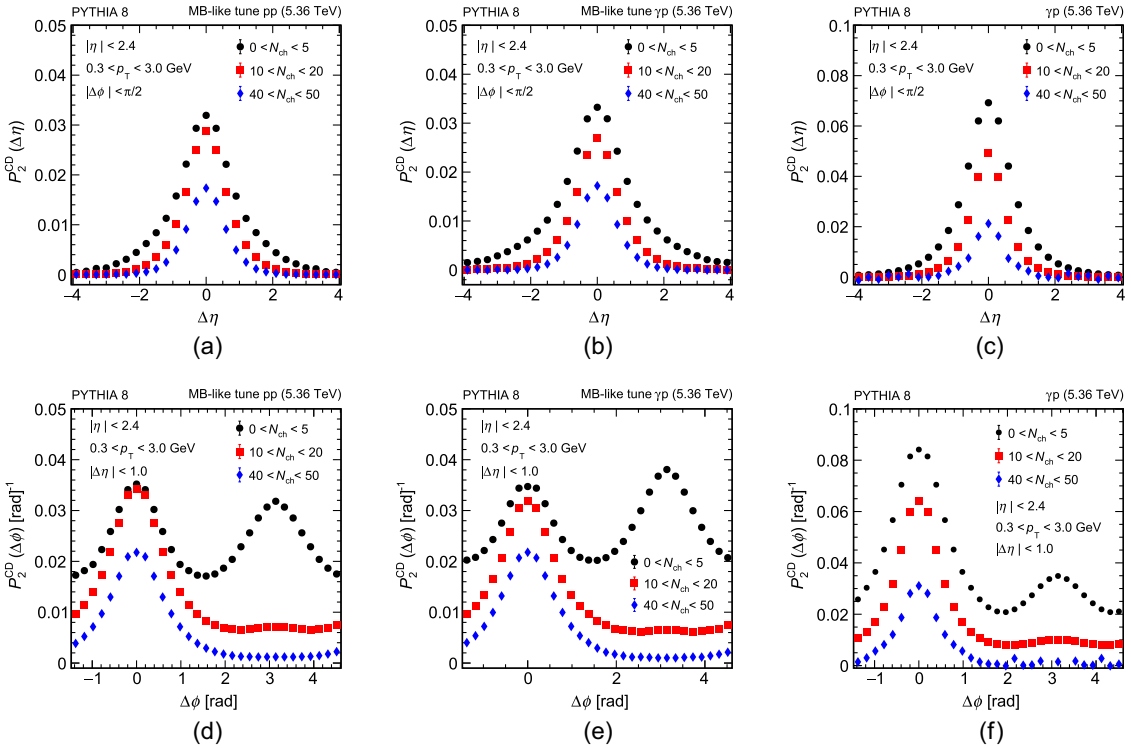


FIG. 6. One-dimensional nearside projection of the momentum balance functions ($P_2^{\rm CD}$) as a function of $\Delta\eta$ (upper panels) and $\Delta\phi$ (lower panels) for three $N_{\rm ch}$ classes in MB-like tune pp (left panels, (a) and (d)), MB-like tune γp (middle panels, (b) and (e)), and γp (right panels, (c) and (f)) collisions at $\sqrt{s} = 5.36$ TeV from PYTHIA 8. The results are obtained in the kinematic region $|\eta| < 2.4$ and $0.3 < p_{\rm T} < 3.0$ GeV for charged hadrons.

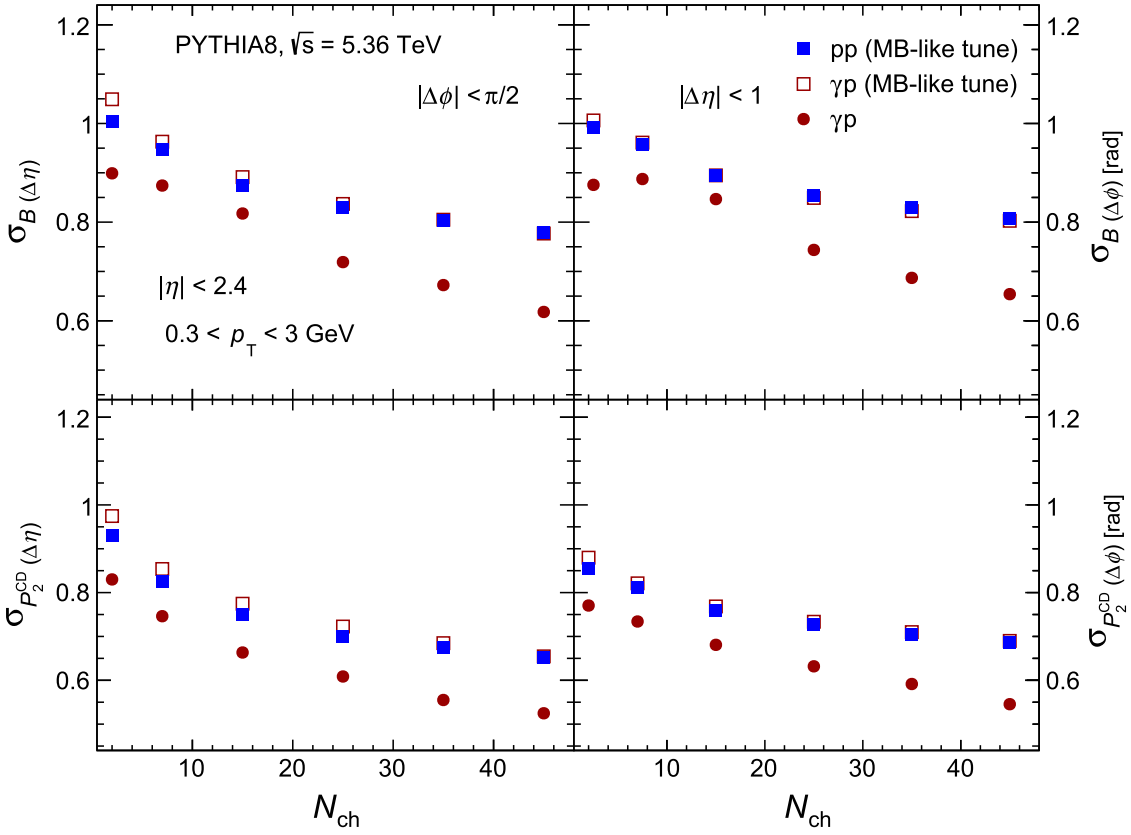


FIG. 7. The RMS width of the number (σ_B) and momentum ($\sigma_{P_2^{\rm CD}}$) of balance functions in terms of $\Delta\eta$ (left column) and $\Delta\phi$ (right column) with $N_{\rm ch}$. Both the trigger and associated particles are considered in $0.3 < p_{\rm T} < 3.0$ GeV and $|\eta| < 2.4$ for the charged hadrons.

Figure 6 presents the 1D projections of $P_2^{\rm CD}$ along the $\Delta\eta$ and $\Delta\phi$ directions. $P_2^{\rm CD}$ shows a clear multiplicity evolution, and their amplitudes gradually decrease with increasing $N_{\rm ch}$. This can be attributed to the combined contribution from $\langle p_{\rm T}\rangle$ weighting and jet-dominated processes, which is more prominent in low-multiplicity pp events. The observed trend in the $P_2^{\rm CD}$ is opposite to the B, and the difference arises between them because $P_2^{\rm CD}$ is not only sensitive to the number of the correlated particle pairs but also to their $p_{\rm T}$ correlations.

C. Width comparison

The strength of the correlation between produced hadron pairs is reflected in the width of the balance functions and is quantified by the observables $\sigma(\Delta\eta)$ and $\sigma(\Delta\phi)$, as defined in Eq. (11). Figure 7 shows a clear multiplicity-dependent trend: the widths of B and $P_2^{\rm CD}$ decrease with increasing $N_{\rm ch}$ for both pp and γp collisions. The trends observed in this study are qualitatively consistent with the available experimental measurements for pp collisions by the ALICE Collaboration [17] despite differences in the kinematic selections, multiplicity definitions, and collision energies. However, both results show similar qualitative behavior on the multiplicity-dependent study of the balance function for charged hadrons. Future measurements in small systems and photon-induced processes at the LHC energies will provide valuable experimental constraints and help further assess the underlying mechanisms responsible for the observed behavior.

The extracted widths of these correlations are smaller in γp collisions than in pp collisions across all multiplicity classes, with the difference becoming more pronounced at higher $N_{\rm ch}$,

$$\sigma^{\gamma p}_{P_2^{\rm CD}(\Delta\eta,\Delta\phi)} \quad \text{or} \quad B(\Delta\eta,\Delta\phi) < \sigma^{pp}_{P_2^{\rm CD}(\Delta\eta,\Delta\phi)} \quad \text{or} \quad B(\Delta\eta,\Delta\phi).$$

A comparison of the widths of the B and $P_2^{\rm CD}$ reveals a clear and systematic dependence on the charged particle multiplicity. The ordering of the widths is preserved across all multiplicity classes,

$$\sigma_{P_2^{\rm CD}(\Delta\eta,\Delta\phi)} < \sigma_{B(\Delta\eta,\Delta\phi)},$$

suggesting that the underlying mechanisms of charge conservation for the balance function and localized jetlike momentum correlations for P_2 remain robust across collision systems. In addition, no significant difference in the extracted widths is observed between γp and pp collisions

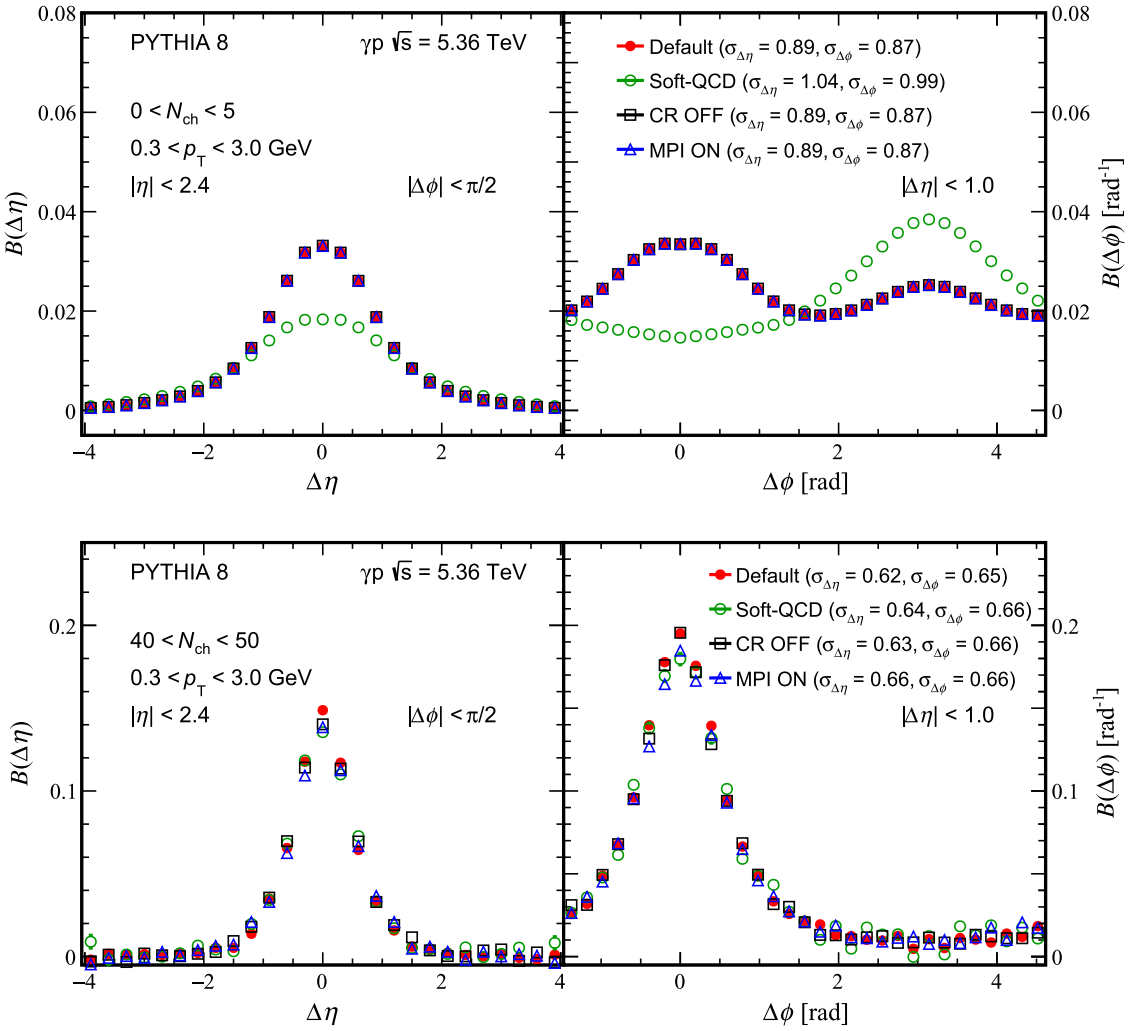


FIG. 8. Balance functions comparison using different PYTHIA 8 configurations. The upper (lower) panels correspond to the multiplicity range $0 < N_{\mathrm{ch}} < 5$ ($40 < N_{\mathrm{ch}} < 50$). The left (right) column presents the $\Delta\eta$ ($\Delta\phi$) balance functions in $0.3 < p_{\mathrm{T}} < 3.0$ GeV and $|\eta| < 2.4$.

when the same PYTHIA 8 configuration is used, despite the different colliding systems. However, a small difference appears at low N_{ch}. These findings highlight a clear picture of multiplicity-driven narrowing in both pp and γp collisions, while this also points to open questions regarding the relative strength of MPI, color reconnection, and hard processes in photon-induced interactions and how these mechanisms scale with event activity in small systems.

To further investigate the sensitivity of balance-function observables to different model configurations, additional studies were performed by varying the CR, MPI, and soft-QCD processes relative to the default configuration used in this study.

Figure 8 presents a comparison of the balance functions $B(\Delta\eta)$ and $B(\Delta\phi)$ for low- and high-multiplicity events in γp collisions. For the low-multiplicity interval ($0 < N_{\mathrm{ch}} < 5$), the soft-QCD-dominated sample exhibits significantly broader balance-function distributions compared to the default one. On the other hand, the CR-OFF and MPI-ON samples remain close to the default prediction. This indicates that soft particle-production processes have a stronger impact on the correlation widths than the individual CR or MPI enabled. At higher multiplicities ($40 < N_{\mathrm{ch}} < 50$), the differences among the various model configurations have smaller effects. A narrower width of the balance functions is found for all the configurations at higher N_{ch} as compared to lower N_{ch}. The similar behavior observed across different PYTHIA 8 configurations at high multiplicity indicates that the narrowing of the balance function is associated with event multiplicity rather than with specific generator tunings used to model particle production mechanisms. However, as this study explores with a limited set of PYTHIA model configurations, these results do not imply that multiplicity is the sole origin of the narrowing behavior but rather are suggestive of its role as a primary contributor.

V. SUMMARY

We present a study of two-particle number (B) and transverse-momentum (P_2^{CD}) balance functions of inclusive charged particles as a function of event multiplicity in γp collisions at LHC energies using PYTHIA 8 simulations and compare the results with pp collisions in the similar multiplicity range. Different PYTHIA 8 configurations are considered, including setups with and without inelastic minimum-bias processes, to quantify the role of MPIs, string-fragmentation based hadronization, and underlying event activities on particle production.

The widths of both correlation observables decrease with increasing multiplicity in both pp and γp collisions, demonstrating a clear multiplicity-dependent narrowing trend. Although photon-induced γp events populate a lower multiplicity range than hadronic pp interactions, the same trend is present. The comparison at given multiplicity isolates the contribution of hard scattering. The low-multiplicity pp events exhibit a pronounced away-side peak driven by back-to-back dijet production, while such contributions are strongly suppressed in γp collisions. A dedicated study with identical minimum-bias configurations for pp and γp collisions shows consistent results, suggesting that the observed multiplicity dependence is closely related to underlying event activity rather than the colliding system and the choice of specific physics processes.

This behavior in γp interactions highlights the importance of future experimental measurements to validate these multiplicity-dependent effects. Future experimental measurements of photon-induced (i.e., γp, γ^{Pb}, γO) collisions will therefore provide a clean environment to separate bulk-dominated nearside correlations at low transverse momentum from jet-driven away-side correlations characteristic of low-multiplicity pp events, delivering a robust baseline for disentangling soft and hard components of particle production across different collision systems.

ACKNOWLEDGMENTS

S. C. Behera and D. Mallick acknowledge the support under the Istituto Nazionale di Fisica Nucleare (INFN) Postdoctoral Fellowship Grants No. B.C. n. 25865 and No. B.C. n. 27077.

DATA AVAILABILITY

The data that support the findings of this article are not publicly available. The data are available from the authors upon reasonable request.

APPENDIX: CHARGE-INDEPENDENT CORRELATIONS

This section presents the charge-independent correlations C_2^{CI} and P_2^{CI} for charged hadrons, calculated as the sum of the SS and OS correlations discussed in Eqs. (7) and (8). Figure 9 shows C_2^{CI} correlations for charged hadrons in MB pp collisions (left column), γp collisions with MB-like

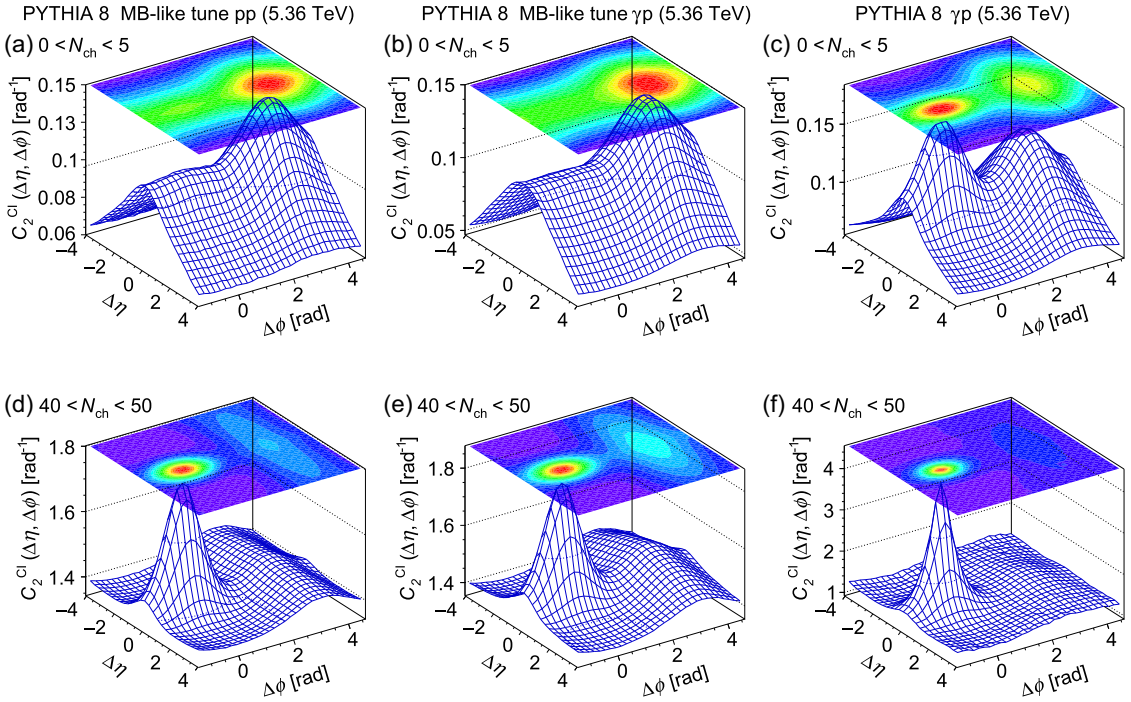


FIG. 9. Two-dimensional charge-independent number correlations (C_2^{CI}) for $0 < N_{\mathrm{ch}} < 5$ (upper panel) and $40 < N_{\mathrm{ch}} < 50$ (lower panel) in MB-like tune pp (left), MB-like tune γp (middle), and γp (right) collisions at $\sqrt{s} = 5.36$ TeV from PYTHIA 8. The results are obtained in the kinematic region $|\eta| < 2.4$ and $0.3 < p_{\mathrm{T}} < 3.0$ GeV charged hadrons.

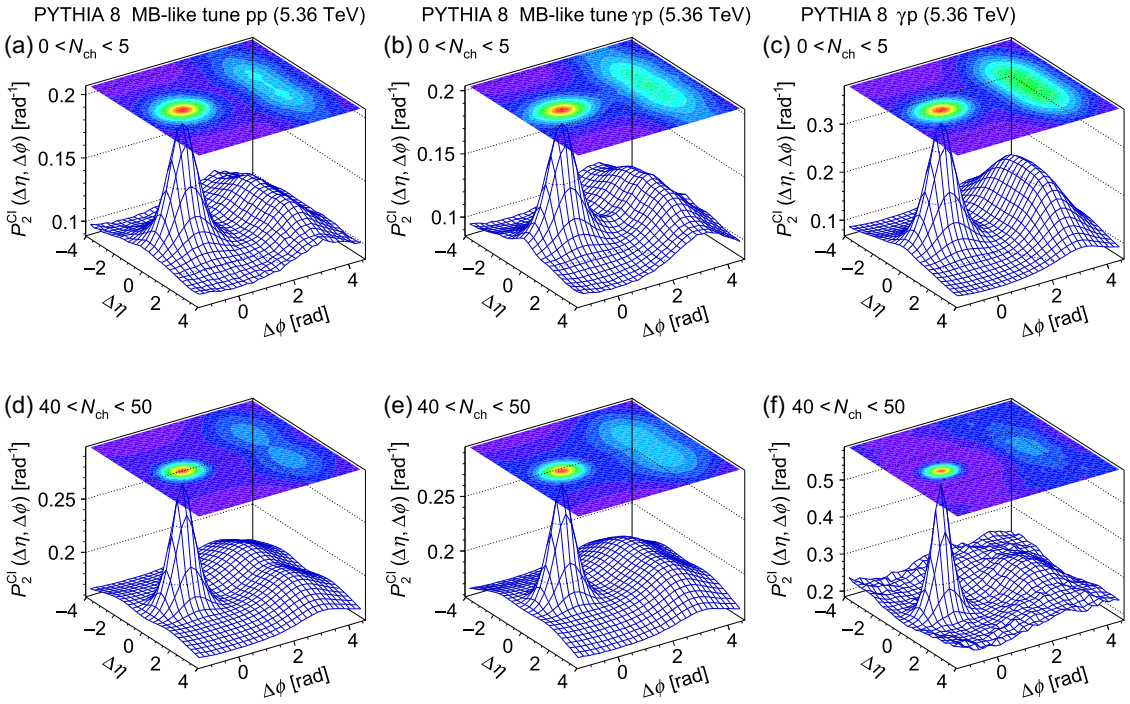


FIG. 10. Two-dimensional charge-independent momentum correlations (P_2^{CI}) for $0 < N_{\mathrm{ch}} < 5$ and $40 < N_{\mathrm{ch}} < 50$ in MB-like tune pp (left), MB-like tune γp (middle), and γp (right) collisions at $\sqrt{s} = 5.36$ TeV from PYTHIA 8. The results are obtained in the kinematic region $|\eta| < 2.4$ and $0.3 < p_{\mathrm{T}} < 3.0$ GeV for charged hadrons.

tune (middle column), and γp collisions (right column) for two N_{ch} classes, $0 < N_{\mathrm{ch}} < 5$ (upper panel) and $40 < N_{\mathrm{ch}} < 50$ (lower panel).

For the low N_{ch}, the near-side CI correlations in MB pp and MB-like γp exhibit relative suppression with respect to γp collisions. This behavior can be attributed to the reduced contribution of short-range correlations and multiparticle interactions. A clear nearside enhancement emerges in all three configurations at higher N_{ch}. The enhancement with multiplicity is associated with a larger contribution from MPI and semihard processes, which strengthen short-range correlations and sharpen the nearside peak; however, the away-side structure becomes relatively suppressed.

Similarly, Fig. 10 presents CI correlations constructed from the transverse momentum components $P_2(\Delta\eta, \Delta\phi)$ for two different event configurations. For low-multiplicity events, all these configurations exhibit a localized nearside peak around $(\Delta\eta, \Delta\phi) \approx (0, 0)$, indicating short-range correlations dominated by jet fragmentation, resonance decays, and local charge conservation. However, the nearside peak in γp collisions is visibly stronger and more sharply localized compared to MB pp and MB-like γp. As the event multiplicity increases, a pronounced enhancement of the nearside peak is observed in both configurations. In contrast, the γp configuration shows a significantly larger peak magnitude and a reduced away-side structure, indicating that the correlations are dominated by hard scattering processes as the $\langle p_{\mathrm{T}} \rangle$ increases.

The CI and CD correlations of C_2 and P_2 are studied for charged hadrons in pp and γp collisions. A similar behavior is observed for both CI and CD results; however, the amplitude of the CI correlations is larger than that of the CD correlations because the CI component includes contributions from both SS and OS pairs. This suggests that the final CI correlation strength arises from various physics processes, such as jet fragmentation, resonance decays, the Hanbury Brown-Twiss effect, LCC, and other global event properties. In addition, the nearside peak of P_2^{CI} is found to be narrower than C_2^{CI}. This behavior is consistent with the angular ordering of the p_{T}, where produced particles exhibit stronger localized momentum correlations. Similar behavior is also expected from hadronic resonance decays as discussed in Refs. [15,16,30].

[1] J. W. Harris and B. Muller, QGP signatures revisited, Eur. Phys. J. C **84**, 247 (2024).

[2] S. Acharya *et al.* (ALICE Collaboration), The ALICE experiment: A journey through QCD, Eur. Phys. J. C **84**, 813 (2024).

[3] A. Hayrapetyan *et al.* (CMS Collaboration), Overview of high-density QCD studies with the CMS experiment at the LHC, Phys. Rep. **1115**, 219 (2025).

[4] I. Arsene *et al.* (BRAHMS Collaboration), Quark gluon plasma and color glass condensate at RHIC? The Perspective from the BRAHMS experiment, Nucl. Phys. **A757**, 1 (2005).

[5] J. Adams *et al.* (STAR Collaboration), Experimental and theoretical challenges in the search for the quark gluon plasma: The STAR Collaboration's critical assessment of the evidence from RHIC collisions, Nucl. Phys. **A757**, 102 (2005).

[6] ALICE Collaboration, Future high-energy pp programme with ALICE, https://cds.cern.ch/record/2724925, Report No ALICE-PUBLIC-2020-005.

[7] B. B. Back *et al.* (PHOBOS Collaboration), The PHOBOS perspective on discoveries at RHIC, Nucl. Phys. **A757**, 28 (2005).

[8] P. Kovtun, D. T. Son, and A. O. Starinets, Viscosity in strongly interacting quantum field theories from black hole physics, Phys. Rev. Lett. **94**, 111601 (2005).

[9] H. Song, S. A. Bass, U. Heinz, T. Hirano, and C. Shen, 200 A GeV Au + Au collisions serve a nearly perfect quark-gluon liquid, Phys. Rev. Lett. **106**, 192301 (2011).

[10] J. Adam *et al.* (ALICE Collaboration), Multiplicity and transverse momentum evolution of charge-dependent correlations in pp, p–Pb, and Pb–Pb collisions at the LHC, Eur. Phys. J. C **76**, 86 (2016).

[11] S. Pratt, General charge balance functions, A tool for studying the chemical evolution of the quark-gluon plasma, Phys. Rev. C **85**, 014904 (2012).

[12] S. A. Bass, P. Danielewicz, and S. Pratt, Clocking hadronization in relativistic heavy ion collisions with balance functions, Phys. Rev. Lett. **85**, 2689 (2000).

[13] S. Pratt, Identifying the charge carriers of the quark-gluon plasma, Phys. Rev. Lett. **108**, 212301 (2012).

[14] S. C. Behera and A. Khuntia, Jet-associated balance functions of charged and identified hadrons in pp collisions at $\sqrt{s} = 13.6$ TeV using PYTHIA, Phys. Rev. D **113**, 032008 (2026).

[15] S. Acharya *et al.* (ALICE Collaboration), Measurements of differential two-particle number and transverse momentum correlation functions in pp collisions at $\sqrt{s} = 13$ TeV, Eur. Phys. J. C **85**, 866 (2025).

[16] S. Acharya *et al.* (ALICE Collaboration), Two particle differential transverse momentum and number density correlations in p–Pb and Pb-Pb at the LHC, Phys. Rev. C **100**, 044903 (2019).

[17] J. Adam *et al.* (ALICE Collaboration), Multiplicity and transverse momentum evolution of charge-dependent correlations in pp, p–Pb, and Pb–Pb collisions at the LHC, Eur. Phys. J. C **76**, 86 (2016).

[18] M. M. Aggarwal *et al.* (STAR Collaboration), Balance functions from Au + Au, d + Au, and $p + p$ collisions at $\sqrt{s_{\rm NN}} = 200$ GeV, Phys. Rev. C **82**, 024905 (2010).

[19] A. Tumasyan *et al.* (CMS Collaboration), Multiplicity and transverse momentum dependence of charge-balance functions in pPb and PbPb collisions at LHC energies, J. High Energy Phys. 08 (2024) 148.

[20] B. Abelev *et al.* (ALICE Collaboration), Charge correlations using the balance function in Pb-Pb collisions at $\sqrt{s_{NN}} = 2.76$ TeV, Phys. Lett. B **723**, 267 (2013).

[21] C. Pruneau, V. Gonzalez, B. Hanley, A. Marin, and S. Basu, Accounting for nonvanishing net-charge with unified balance functions, Phys. Rev. C **107**, 014902 (2023).

[22] C. A. Pruneau, Role of baryon number conservation in measurements of fluctuations, Phys. Rev. C **100**, 034905 (2019).

[23] S. Acharya *et al.* (ALICE Collaboration), General balance functions of identified charged hadron pairs of (π,K,p) in Pb–Pb collisions at $\sqrt{s_{NN}} = 2.76$ TeV, Phys. Lett. B **833**, 137338 (2022).

[24] V. Khachatryan *et al.* (CMS Collaboration), Observation of long-range near-side angular correlations in proton-proton collisions at the LHC, J. High Energy Phys. 09 (2010) 091.

[25] V. Khachatryan *et al.* (CMS Collaboration), Measurement of long-range near-side two-particle angular correlations in pp collisions at $\sqrt{s} = 13$ TeV, Phys. Rev. Lett. **116**, 172302 (2016).

[26] Y. C. Chen *et al.* (Belle Collaboration), Measurement of two-particle correlations of hadrons in e^+e^- collisions at belle, Phys. Rev. Lett. **128**, 142005 (2022).

[27] S. Chatrchyan *et al.* (CMS Collaboration), Long-range and short-range dihadron angular correlations in central PbPb collisions at $\sqrt{s_{\rm NN}} = 2.76$ TeV, J. High Energy Phys. 07 (2011) 076.

[28] S. Chatrchyan *et al.* (CMS Collaboration), Observation of long-range, near-side angular correlations in pPb collisions at the LHC, Phys. Lett. B **718**, 795 (2013).

[29] S. Acharya *et al.* (ALICE Collaboration), Emergence of long-range angular correlations in low-multiplicity proton-proton collisions, Phys. Rev. Lett. **132**, 172302 (2024).

[30] S. C. Behera and A. Khuntia, Two-particle number and transverse momentum balance function with event-topology in pp collisions at $\sqrt{s} = 13$ TeV, Phys. Rev. D **114**, 036025 (2026).

[31] S. C. Behera and A. Khuntia, System size and event shape dependence of particle-identified balance functions in proton-proton collisions at $\sqrt{s} = 13$ TeV, Phys. Rev. C **113**, 035201 (2026).

[32] B. Sahoo, B. K. Nandi, P. Pujahari, S. Basu, and C. Pruneau, Simulation studies of $R_2(\Delta\eta, \Delta\phi)$ and $P_2(\Delta\eta, \Delta\phi)$ correlation functions in pp collisions with the PYTHIA and HERWIG models, Phys. Rev. C **100**, 024909 (2019).

[33] C. Bierlich *et al.*, A comprehensive guide to the physics and usage of PYTHIA 8.3, SciPost Phys. Codebases **2022**, 8 (2022).

[34] A. Tumasyan *et al.* (CMS Collaboration), CMS PYTHIA 8 colour reconnection tunes based on underlying-event data, Eur. Phys. J. C **83**, 587 (2023).

[35] A. Tumasyan *et al.* (CMS Collaboration), Two-particle azimuthal correlations in γp interactions using pPb collisions at $\sqrt{s_{\mathrm{NN}}} = 8.16$ TeV, Phys. Lett. B **844**, 137905 (2023).

[36] G. Aad *et al.* (ATLAS Collaboration), Two-particle azimuthal correlations in photonuclear ultraperipheral Pb + Pb collisions at 5.02 TeV with ATLAS, Phys. Rev. C **104**, 014903 (2021).

[37] C. Bierlich *et al.*, A comprehensive guide to the physics and usage of PYTHIA 8.3, SciPost Phys. Codebases **2022**, 8 (2022).

[38] I. Helenius and M. Utheim, Hadron-ion collisions in PYTHIA and the vector-meson dominance model for photoproduction, Eur. Phys. J. C **84**, 1155 (2024).